Supplement of Geosci. Model Dev., 12, 4603–4625, 2019
https://doi.org/10.5194/gmd-12-4603-2019-supplement

Geoscientific Model Development
Open Access
EGU

Supplement of

Multimodel simulations of a springtime dust storm over northeastern China: implications of an evaluation of four commonly used air quality models (CMAQ v5.2.1, CAMx v6.50, CHIMERE v2017r4, and WRF-Chem v3.9.1)

Siqi Ma et al.

Correspondence to: Xuelei Zhang (zhangxuelei@neigae.ac.cn) and Daniel Q. Tong (qtong@gmu.edu)

S1 Dust emission schemes in air quality models

S1.1 GOCART dust scheme in WRF-Chem v3.9.1

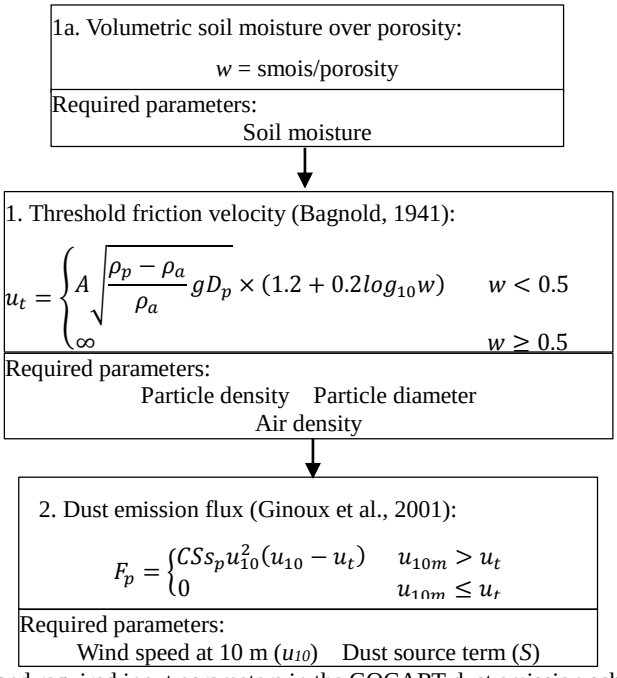

Figure S1. Schematic diagram and required input parameters in the GOCART dust emission scheme in WRF-Chem v3.9.1.

Table S1. Variable list for the GOCART dust emission scheme in WRF-Chem v3.9.1

Variable	Name	Value	Variable	Name	Value
smois	Soil moisture	Variable field	D_p	Particle diameter	Variable
porosity	Soil porosity	Constant field	u_{10}	Wind speed at 10 m	Variable field
w	Volumetric soil moisture over porosity	Variable field	u_t	Threshold wind speed	Variable field
A	Dimensionless tuning parameter	0.13	C	Dimensional constant	1 mg s^2 m^{-5}
ρ_p	Particle density	2.5–2.65 g cm^{-3}	S	Dust source strength function	Variable field
ρ_a	Air density	Variable field	s_p	Soil surface mass fraction	Variable field

S1.2 AFWA dust scheme in WRF-Chem v3.9.1

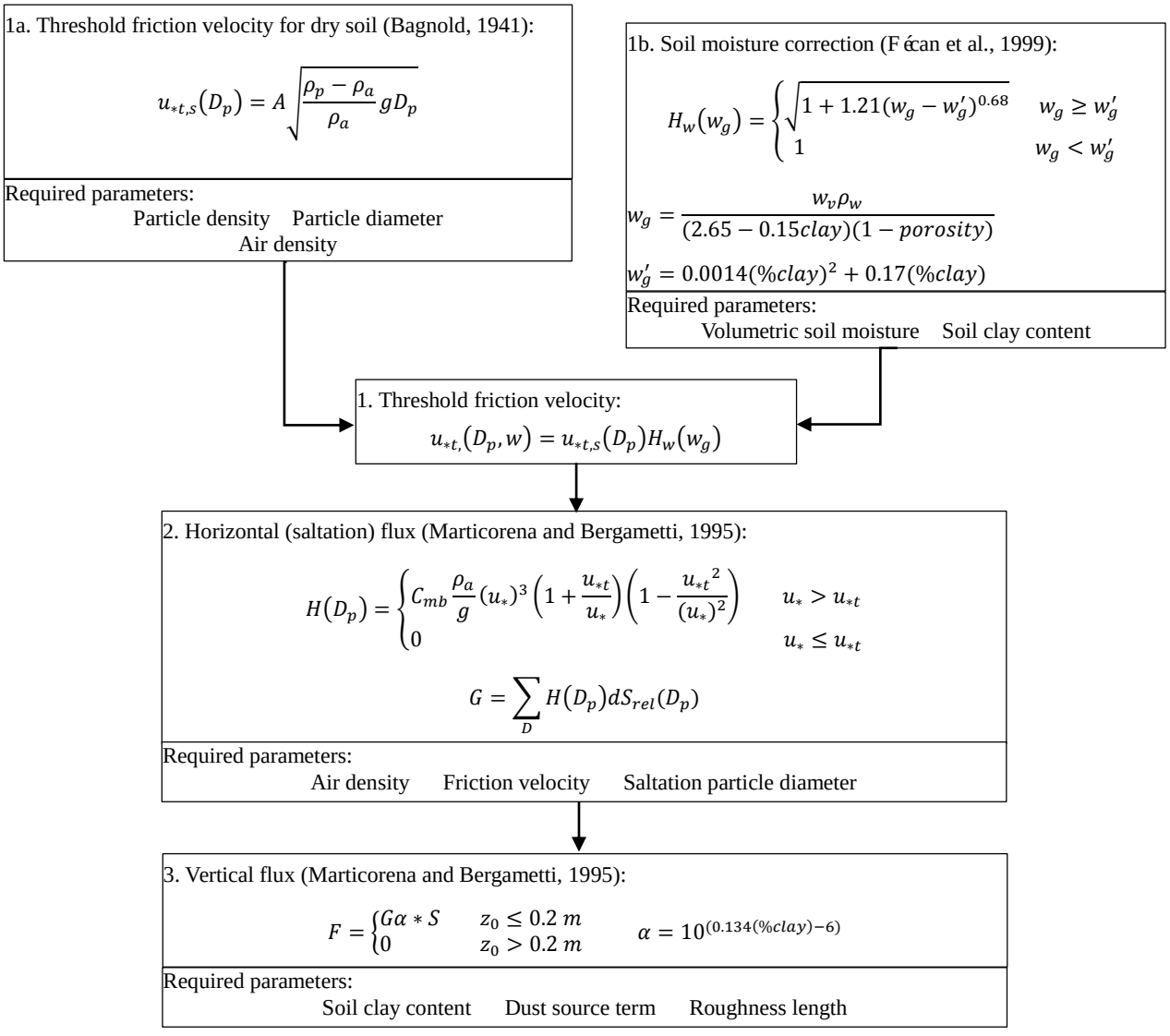

Figure S2. Schematic diagram and required input parameters in the AFWA dust emission scheme in WRF-Chem v3.9.1.

Table S2. Variable list for the AFWA dust emission scheme in WRF-Chem v3.9.1

Variable	Name	Value	Variable	Name	Value
ρ_p	Particle density	2.5–2.65 g cm^{-3}	w_g'	Moisture without effect on capillary forces	Variable field
ρ_a	Air density	Variable field	w_v	Volumetric soil moisture	Variable field
D_p	Particle diameter	Variable	ρ_w	Water density	1 g cm^{-3}
u_{10}	Wind speed at 10 m	Variable field	c_{smtune}	Soil moisture tuning constant	User set
u_{*t}	Threshold friction velocity	Variable field	c_{ustune}	Friction velocity tuning constant	User set
u_*	Friction velocity	Variable field	*%clay*	Soil clay content mass fraction	Constant field
A	Dimensionless tuning parameter	0.13	C_{mb}	Dimensionless constant	1
w_g	Gravimetric soil moisture	Variable field	S	Dust source strength function	Variable field
α	sandblasting efficiency	Variable field	dSrel	Relative weighting factors for particle size bins	Variable field

S1.3 UOC dust scheme in WRF-Chem v3.9.1

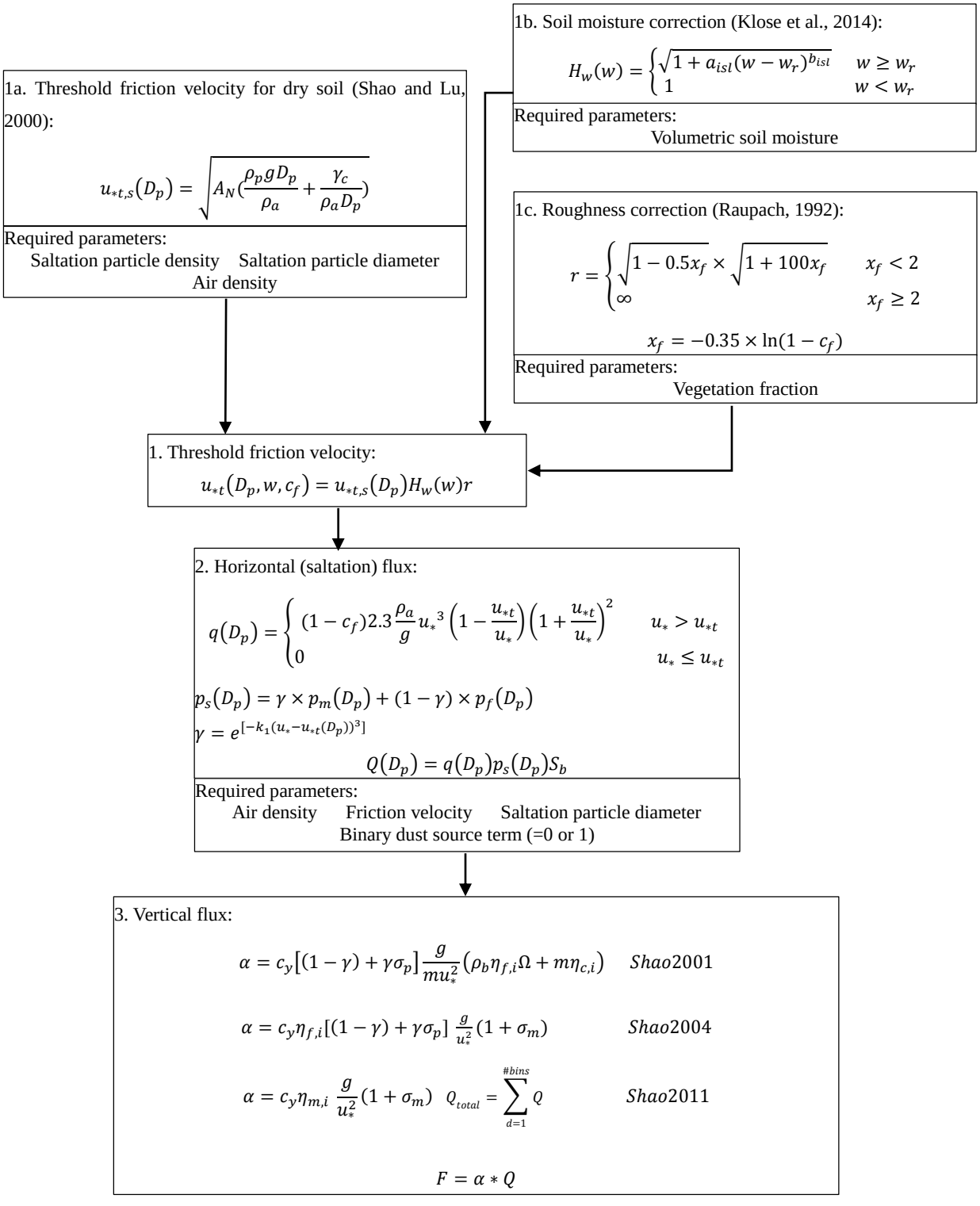

Figure S3. Schematic diagram and required input parameters in the UOC dust emission scheme in WRF-Chem v3.9.1.

Table S3. Variable list for the UOC dust emission scheme in WRF-Chem v3.9.1

Variable	Name	Value	Variable	Name	Value
ρ_p	Particle density	2.5–2.65 g cm^{-3}	c_f	Vegetation fraction	Constant field
ρ_a	Air density	Variable field	p_s	Particle availability term	Variable field
D_p	Particle diameter	Variable	p_m	Minimally disturbed particle size distribution	Variable field
u_{10}	Wind speed at 10 m	Variable field	p_f	Fully disturbed particle size distribution	Variable field
u_{*t}	Threshold friction velocity	Variable field	k_1	Aggregate breakup constant	1
A_N	Dimensionless constant	0.0123	S_b	Binary dust source function	Variable field
γ_c	Dimensional constant	1.65×10^{-4} kg s^{-2}	c_y	Dimensionless constant	0.00001
w	Volumetric soil moisture	Variable field	σ_p	Ratio of particle density to air density	Constant
w_r	Air-dry soil moisture (m^3 m^{-3}) from SOILPARM.TBL	Variable field	σ_m	Revised bombardment efficiency	Variable field
a_{isl}	Empirical constant as a function of soil texture	Constant field	ρ_b	Constant bulk density of the soil	1000 kg m^{-3}
b_{isl}	Empirical constant as a function of soil texture	Constant field	$\eta_{f,i}$	Fully disturbed dust fraction	Variable field
r	Roughness correction factor	Variable field	$\eta_{c,i}$	Soil fraction available for disaggregation	Variable field
x_f	Frontal area index	Variable field	Ω	Bombardment efficiency	Variable field

S1.4 Dust emission scheme in CHIMERE v2017r4

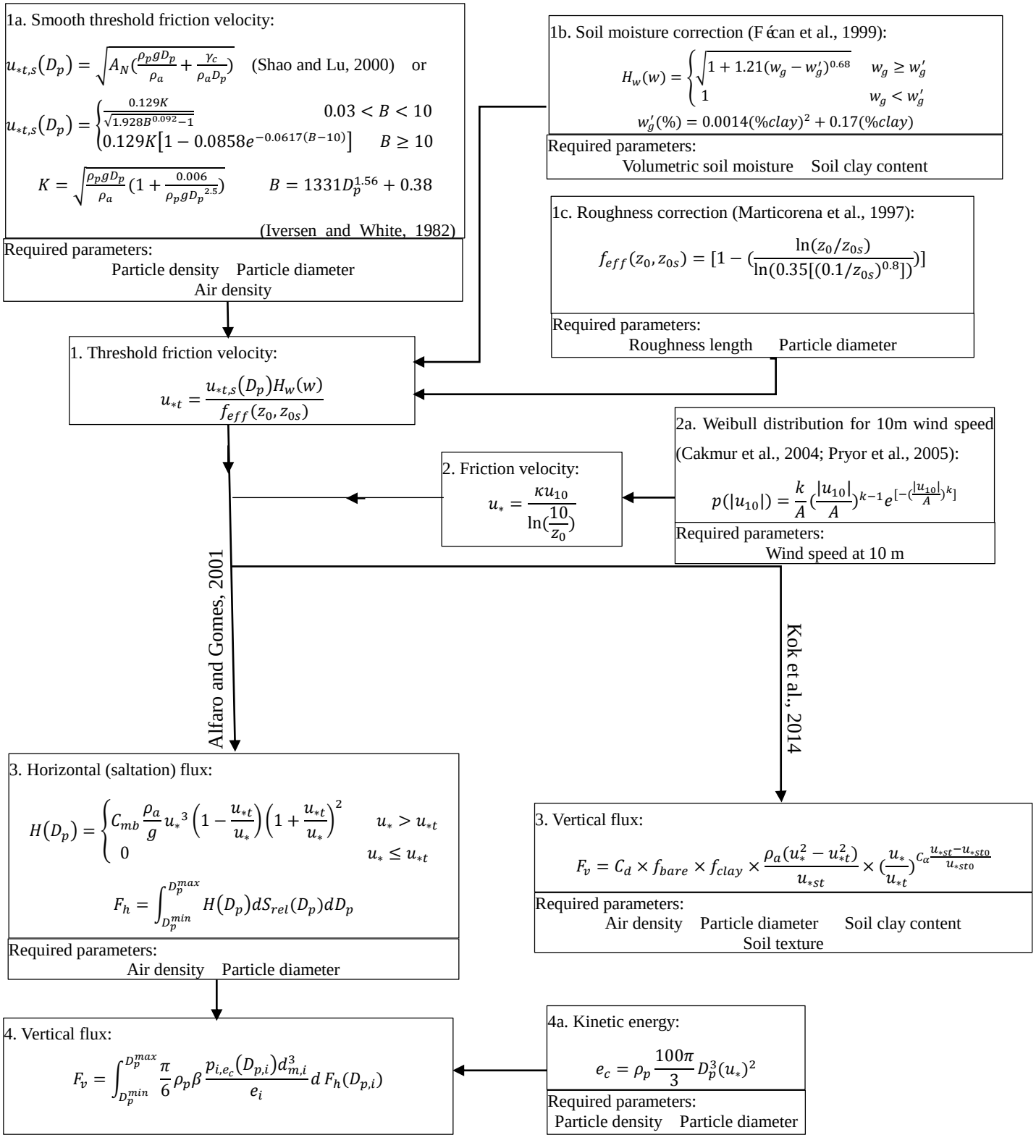

Figure S4. Schematic diagram and required input parameters in the dust emission scheme in CHIMERE v2017r4.

Table S4. Variable list for the dust emission scheme in CHIMERE v2017r4.

Variable	Name	Value	Variable	Name	Value
ρ_p	Particle density	2.5–2.65 g cm^{-3}	$z0s$	"smooth" roughness length	Variable field
ρ_a	Air density	Variable field	κ	von Karman constant	0.4
D_p	Particle diameter	Variable	C_{mb}	Dimensionless constant	1
u_{10}	Wind speed at 10 m	Variable field	$p_{i,ec}$	Fractions of the kinetic energy for the three binding energies	Variable field
u_{*t}	Threshold friction velocity	Variable field	e_i	Binding energies	3.61, 3.52, 3.46
A	mean Modeled wind speed, in meters per second	Variable field	e_c	Kinetic energy	Variable field
k	Dimensionless shape parameter	4	C_d	Dust emission coefficient	Variable field
γ_c	Dimensional constant	1.65×10^{-4} kg s^{-2}	f_{bare}	Fraction of the surface that consists of bare soil	Constant field
w_g	Gravimetric soil moisture	Variable field	f_{clay}	Soil clay content mass fraction	Constant field
w_g'	Moisture without effect on capillary forces	Variable field	u_{*st}	Friction velocity for a standard atmospheric density	Variable field
$z0$	"aeolian" roughness length	Variable field	u_{*st0}	u_{*st} for an optimally erodible soil	0.16 m s^{-1}
A_N	Dimensionless constant	0.0123	C_α	Dimensionless constant	2.7

S1.5 Dust emission scheme in CMAQ v5.2.1

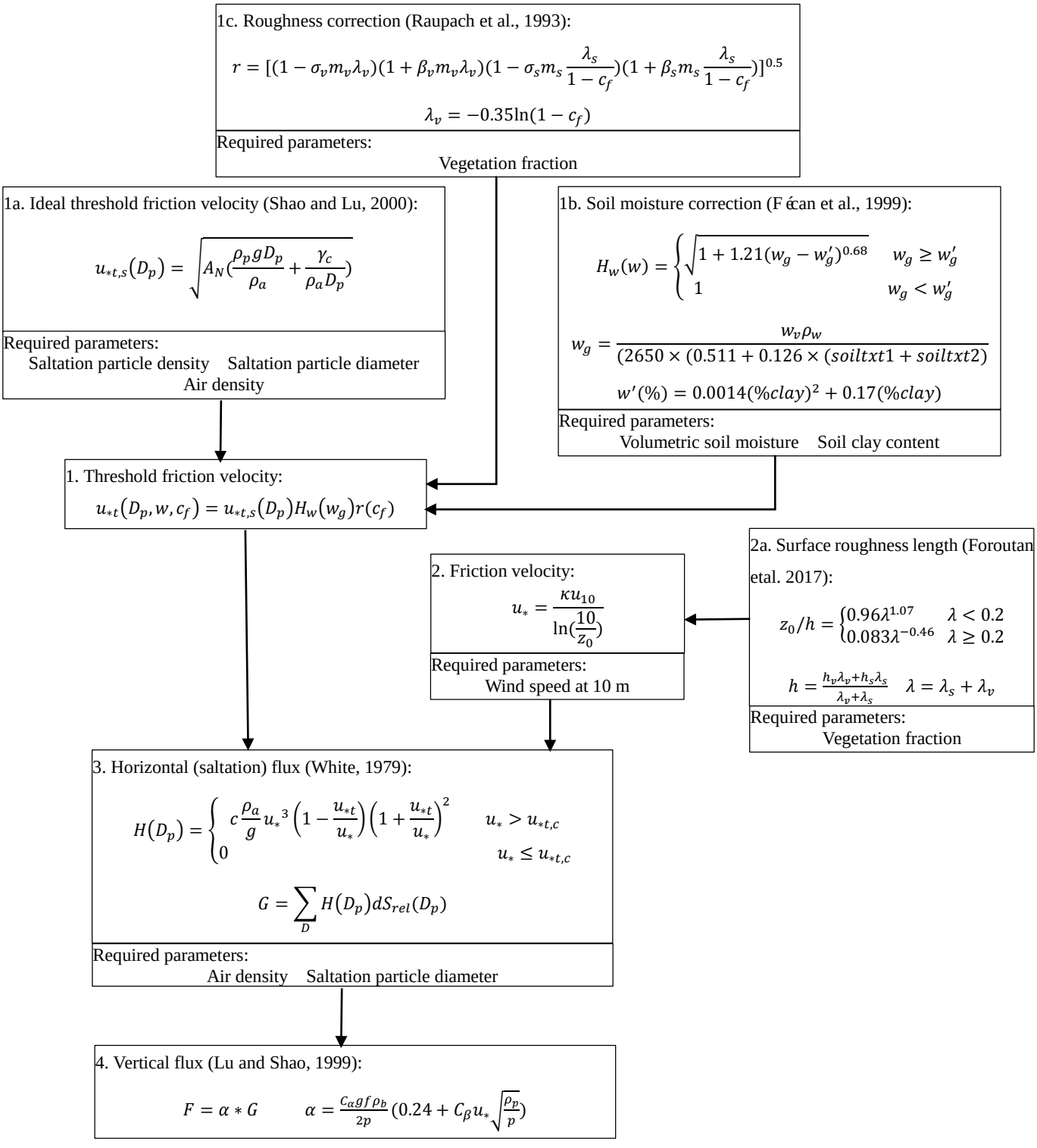

Figure S5. Schematic diagram and required input parameters in the dust emission scheme in CMAQ v5.2.1.

Table S5. Variable list for the dust emission scheme in CMAQ v5.2.1.

Variable	Name	Value	Variable	Name	Value
ρ_p	Particle density	2.5–2.65 g cm^{-3}	m_s	Coefficient	0.5
ρ_a	Air density	Variable field	β_s	Coefficient	90
D_p	Particle diameter	Variable	c_f	Vegetation fraction	Constant field
u_{10}	Wind speed at 10 m	Variable field	κ	von Karman constant	0.4
u_{*t}	Threshold friction velocity	Variable field	z_0	Surface roughness length	Variable field
A_N	Dimensionless constant	0.0123	h	Effective height of roughness elements	Variable field
γ_c	Dimensional constant	1.65×10^{-4} kg s^{-2}	h_v	Height of solid element	Constant field
w_g	Gravimetric soil moisture	Variable field	h_s	Height of vegetation element	Constant field
w_g'	Moisture without effect on capillary forces	Variable field	c	Dimensionless constant	1
w_v	Volumetric soil moisture	Variable field	α	Sandblasting efficiency	Variable field
r	Roughness correction factor	Variable field	C_α	Dimensionless coefficient	0.0002~0.001
σ_v	Coefficient	1.45	C_β	Dimensionless coefficient	2.09
m_v	Coefficient	0.16	f	Fraction of fine particles contained in the soil volume	Variable field
λ_v	Roughness densities based on vegetation elements	Variable field	p	Plastic pressure	Variable field
λ_s	Roughness densities based on solid elements	Constant field	ρ_b	Bulk soil density	1000 kg m^{-3}
λ	Total roughness density	Variable field	ρ_p	Soil particle density	2650 kg m^{-3}
β_v	Coefficient	202	*soiltxt1*	the amount of coarse sand in each soil type	Constant field
σ_s	Coefficient	1	*soiltxt2*	the amount of fine-medium sand sand in each soil type	Constant field

S1.6 Dust emission scheme in CAMx v6.50

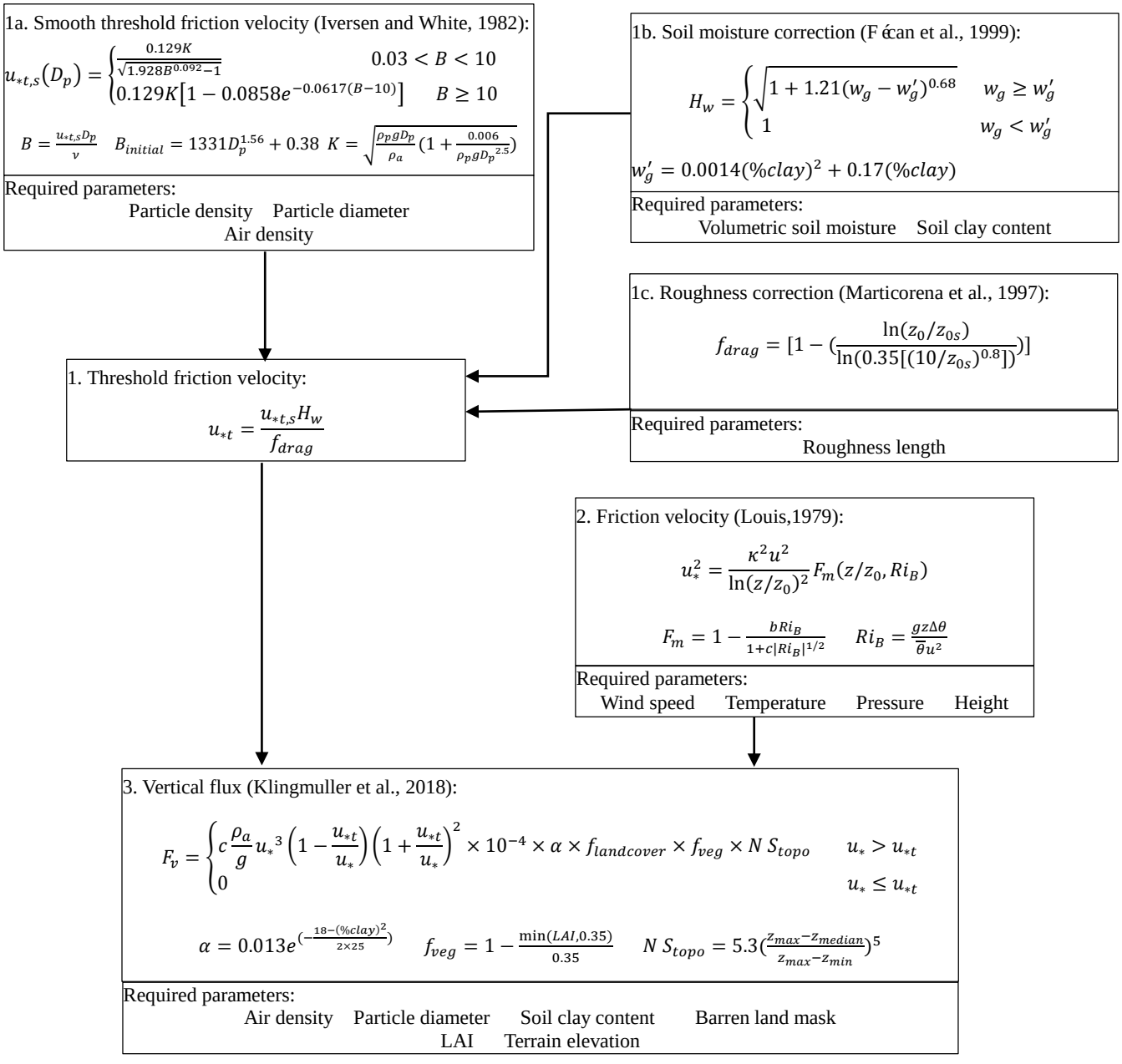

Figure S6. Schematic diagram and required input parameters in the dust emission scheme in CAMx v6.50.

Table S6. Variable list for the dust emission scheme in CAMx v6.50.

Variable	Name	Value	Variable	Name	Value
ρ_p	Particle density	2.5–2.65 g cm^{-3}	κ	von Karman constant	0.4
ρ_a	Air density	Variable field	c	Empirical constant	1.5
D_p	Particle diameter	Variable	α	sandblasting efficiency	Variable field
u	Wind speed at heihgt z	Variable field	*%clay*	Soil clay content mass fraction	Constant field
θ	Potential temperature at height z	Variable field	$f_{landcover}$	Barren land mask	Constant field
R_{iB}	Richardson number	Variable field	f_{veg}	Vegetation factor	Variable field
u_{*t}	Threshold friction velocity	Variable field	*LAI*	Leaf area index	Variable field
A_N	Dimensionless constant	0.0123	N	Normalisation factor	5.3
γ_c	Dimensional constant	1.65×10^{-4} kg s^{-2}	S_{topo}	Topography factor	Variable field
w_g	Gravimetric soil moisture	Variable field	z_{max}	Maximum elevation in the surrounding circle with 10 ° diameter	Variable field
w_g'	Moisture without effect on capillary forces	Variable field	z_{min}	Minimum elevation in the surrounding circle with 10 ° diameter	Variable field
z_0	“aeolian” roughness length	0.01	z_{median}	Median elevation in a circle with 1 °diameter	Variable field
z_{0s}	“smooth” roughness length	0.00333	v	Air kinematic viscosity	Variable field

S2 Comparison of wind speed with different land surface schemes in WRF

The modeling results showed the wind speed of two schemes changed similarly while their differences often appeared near the extreme values and generally larger than measurements (Fig. S7). The mean root mean square error (RMSE) between two schemes and measurements were 1.52 m s^{-1} (for Noah-MP scheme) and 1.61 m s^{-1} (for Pleim-Xiu scheme) respectively and the differences could not pass the significance t-test. Their correlation coefficients were both 0.8, passing the significance test at 0.01 level. These comparisons showed close results between two schemes, however, the errors of Noah scheme in eight monitoring sites had a larger standard deviation showing higher dispersion than PX scheme. Therefore in the following study, the physical parameterization schemes used in the WRF model were WRF Double-Moment 6-class microphysics scheme, the Rapid Radiative Transfer Model for GCMs (RRTMG) longwave and shortwave radiation scheme, Pleim-Xiu scheme for surface layer and land-surface scheme, ACM2 (Pleim) boundary layer scheme, and Grell-Devenyi ensemble cumulus scheme.

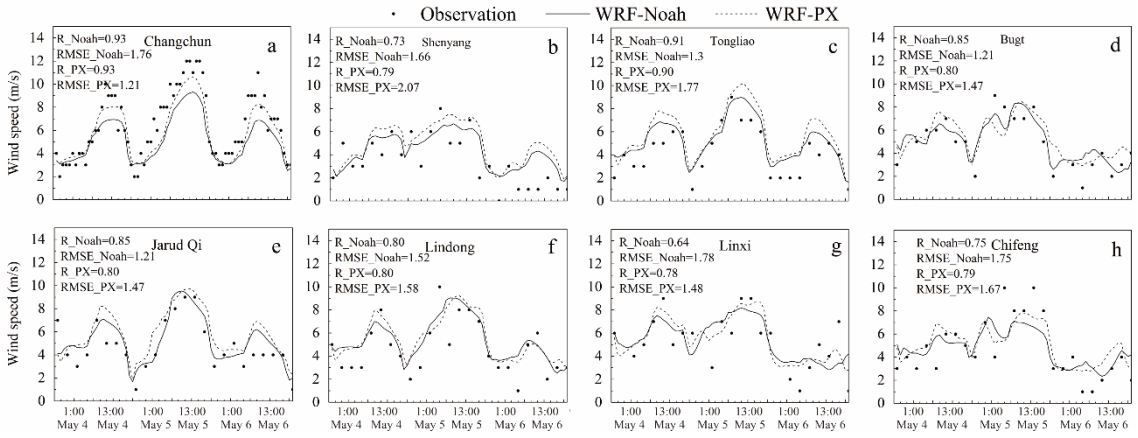

Figure S7. Wind speed hourly variations and the correlation coefficient between observation and WRF simulation with land surface scheme of Noah and Pleim-Xiu respectively wind speed in each site (WRF-Noah indicated the simulating results with Noah land surface scheme while WRF-PX indicated the results with Pleim-Xiu, the observation wind speed were hourly data in Changchun station while in other sites were available every 3 h.)

S3 Dust mask in CAMx model

The dust mask map used in CAMx, which is similar to the dust source map, only has two values: 0 indicating no erodible dust potential while 1 dust emitting capacity in the grid cell. Dust flux will be calculated with the clay fraction-dependent vertical-to-horizontal dust flux ratio (Fig. S8a). However, no dust erodible area was recorded for the region of Northeastern China in this dust mask file (Fig. S8b). Therefore, no further evaluation was conducted for the dust emission scheme in CAMx.

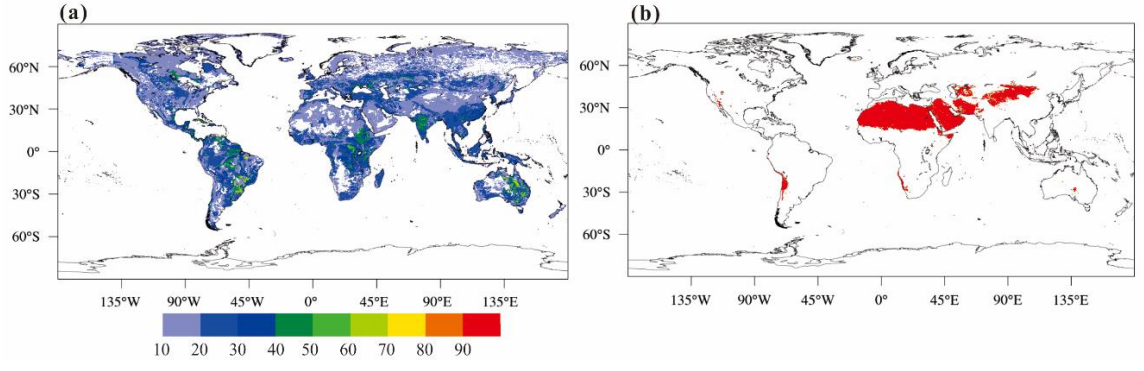

Figure S8. The global distribution of clay fraction (%) in top 4.5 cm soil layer (**a**) and dust mask (**b**).

S4 Performance of WRF-Chem dust simulation with Noah land surface scheme

We conducted the dust emission modeling with the land surface model (LSM) of Noah and find that the simulated dust concentrations are much lower than those derived from PX scheme (Fig. S9). We further compared u_*, U10 and surface soil moisture calculated via PX and Noah scheme and the temporal variations of them are provided in Fig. S10. It shows that the variation curves of u_* are quite similar and it does not present a stronger U-u_* conversion in the PX/ACM2 setting than in Noah scheme over the research area at this time. By contrast, the Noah surface soil moisture shows large difference from PX, with

values 93.6% higher in Changchun City and 29.6% higher in the NEC area (Table S7). Moreover, the soil moisture curve with two LSM schemes are quite different. These discrepancies may result in the differences of estimated dust emissions. The lower soil moisture (which makes smaller threshold friction velocity) simulated by using PX scheme could be the reason of the stronger dust emission magnitude from PX compared to Noah LSM scheme.

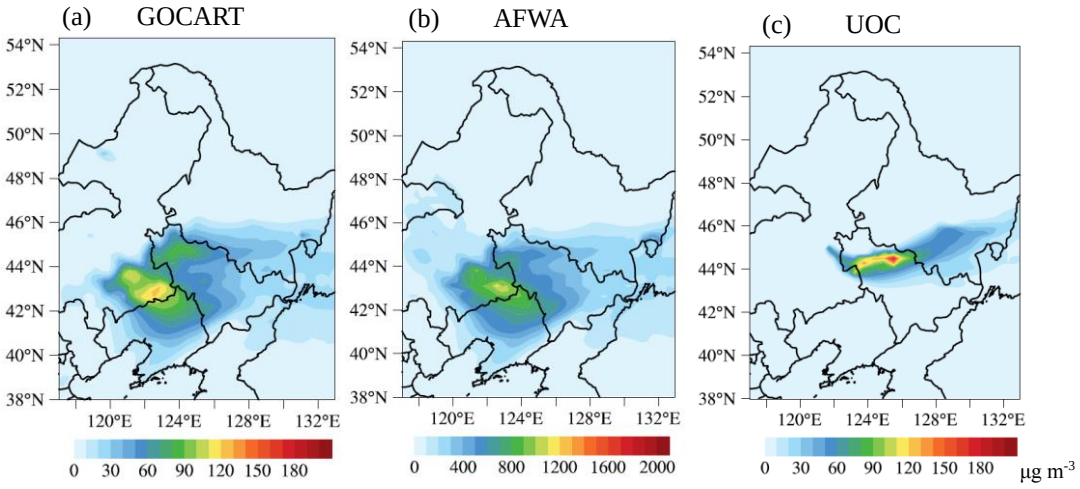

Figure S9. Daily mean PM_{10} distributions in NEC on May 5th, 2015 using GOCART, AFWA and UOC with LSM of Noah.

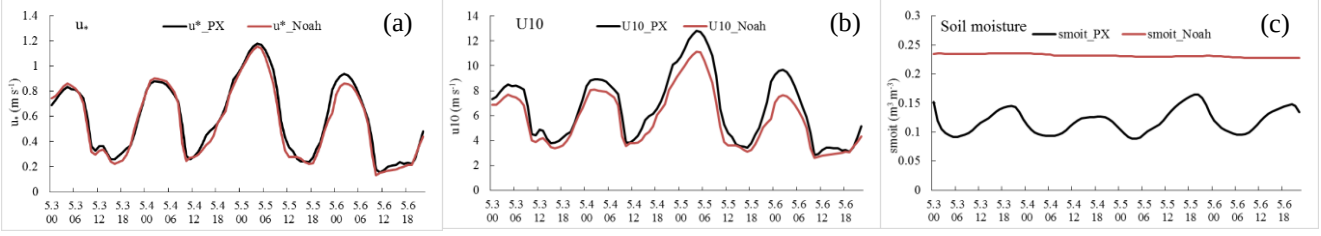

Figure S10. Time series of u_*, U10 and surface soil moisture simulated via LSM of PX and Noah in Changchun City during the dust episode.

Table S7. Mean u_*, U10 and surface soil moisture simulated via LSM of PX and Noah in the research area of NEC

	PX	NOAH
u_* (m s^{-1})	5.10	4.66
U10 (m s^{-1})	0.51	0.46
soil moisture (m^3 m^{-3})	0.27	0.35

S5 Friction velocity and threshold friction velocity

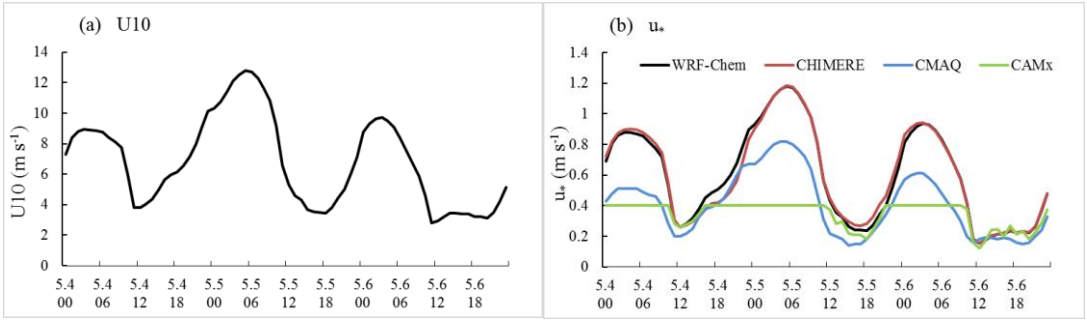

Figure S11. Time series of U10 (a), and u_* (b) from WRF-Chem, CHIMERE, CMAQ and CAMx in Changchun City during the dust episode.

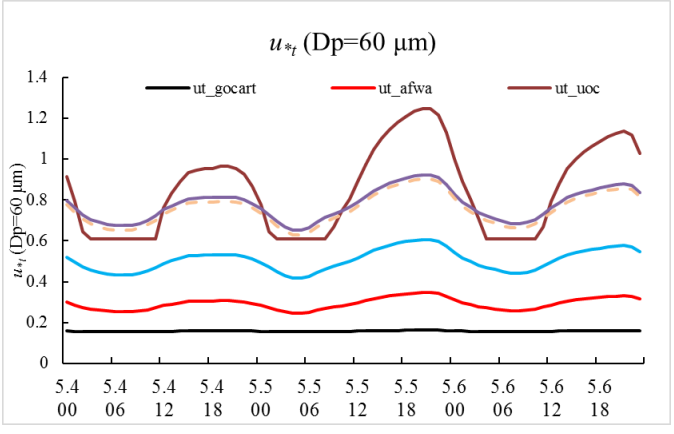

Figure S12. Time series of u_{*t} in from dust emission model of GOCART WRF-Chem, AFWA WRF-Chem, UOC WRF-Chem, CHIMERE, CMAQ and CAMx in Changchun City during the dust episode.

S6 Inter-model Comparisons

The correlation coefficients, biases and errors between simulations with each dust scheme and observations in four sub-areas are quite different. Generally, the simulations performed the best in the sub-area of CTA while showed lowest CORR in NWA. For the 12 simulations, UOC_Shao2004 (s04 in Table S2) yielded the highest CORR values, of up to 0.82, among the four dust schemes in WRF-Chem, and the UOC simulation with dust source map G12_0.1_seasonal (g12 in Table S2) showed the strongest correlation of all. CHIMERE and CMAQ yielded CORR values ranging from 0.43 to 0.76, with good correlations in all three areas. Although the CORRs of WRF-Chem with GOCART were the lowest among all schemes, that combination yielded very low NSDs and RMSEs, showing that simulated concentrations were closer to the measurements. AFWA yielded relatively low NSDs and RMSEs in CTA and NEA, but the highest values in sub-area SWA. UOC_Shao2004 in CTA and NEA yielded the highest deviations. The NMBs and NMEs of the WRF-Chem simulations were lower in the CTA and SWA sub-areas than in the other two sub-areas. Finally, CHIMERE yielded the lowest NMB (near zero) and an NME <75%, while the NMB and NME for CMAQ were slightly larger.

Table S8 Statistic parameters for each simulation

Region	Parameter	chem_goc art_g01	chem_goc art_k08	chem_gocar t_g12	chem_afw a_g01	chem_afw a_k08	chem_afwa _g12

CTA	CORR	0.27	0.46	0.64	0.73	0.63	0.79	
	RMSE	245.76	291.63	191.67	291.52	237.43	169.07	
	NMB	-0.18	1.13	0.12	1.34	0.92	0.38	
	NME	79.11	160.16	66.45	146.88	116.00	64.81	
	BIAS	-46.64	160.16	1.48	208.02	129.50	49.12	
	NSD	0.36	1.09	0.48	2.62	1.32	1.33	
SWA	CORR	0.21	0.15	0.35	0.38	0.17	0.46	
	RMSE	101.37	129.51	89.26	186.82	111.39	112.87	
	NMB	0.06	0.41	0.26	1.24	0.23	0.54	
	NME	71.66	45.91	62.71	142.18	70.43	79.06	
	BIAS	1.84	45.91	22.55	130.20	26.86	52.59	
	NSD	0.89	1.71	1.14	3.74	1.21	2.48	
NEA	CORR	0.28	0.49	0.71	0.53	0.53	0.78	
	RMSE	188.16	229.21	136.18	200.94	242.70	110.43	
	NMB	-0.72	1.59	-0.24	0.99	1.55	-0.03	
	NME	76.59	155.32	57.13	135.47	180.73	52.07	
	BIAS	-93.81	155.32	-37.37	103.45	154.54	-9.10	
	NSD	0.04	0.96	0.17	1.23	1.76	0.50	
NWA	CORR	0.30	0.10	0.33	0.19	0.17	0.42	
	RMSE	34.10	206.11	35.79	155.95	192.70	39.83	
	NMB	-0.55	5.35	0.35	3.58	4.54	0.34	
	NME	63.31	173.97	70.81	374.11	464.72	74.77	
	BIAS	-18.91	173.97	14.42	119.80	147.57	15.32	
	NSD	0.24	48.62	1.28	38.74	70.17	2.47	

Region	Parameter	chem_s04_g01	chem_s04_k08	chem_s04_g12	chim_iegrod3	cmaq	cmaq_agland	camx
CTA	CORR	0.68	0.76	0.76	0.73	0.77	0.71	0.57
	RMSE	534.95	210.93	232.37	179.84	232.18	303.64	187.89
	NMB	-0.17	-0.07	1.56	0.10	0.16	0.45	0.12
	NME	126.11	68.59	72.02	63.72	68.61	84.86	67.95
	BIAS	61.35	-49.36	-22.97	4.61	7.49	60.39	-1.14
	NSD	12.24	1.63	2.43	1.04	2.31	3.89	0.36
SWA	CORR	0.42	0.47	0.46	0.51	0.45	0.43	0.18
	RMSE	127.89	97.92	92.97	104.79	151.89	191.91	138.79
	NMB	-0.63	-0.51	1.25	0.34	0.59	0.94	1.06
	NME	77.00	69.43	65.40	68.83	87.60	110.08	124.62
	BIAS	-20.24	-66.08	-53.47	31.60	56.07	92.57	100.93
	NSD	3.32	0.44	0.82	3.42	4.20	5.87	0.63
NEA	CORR	0.60	0.78	0.81	0.62	0.71	0.67	0.74
	RMSE	227.96	319.06	266.62	156.00	143.50	139.10	115.85
	NMB	0.97	0.54	2.24	-0.53	-0.19	-0.05	0.00
	NME	95.36	134.61	102.22	66.09	68.48	66.53	55.11
	BIAS	-12.75	75.70	39.01	-62.59	55.05	56.91	-8.26
	NSD	3.28	8.02	6.09	0.16	0.12	0.21	0.42
NWA	CORR	0.53	0.38	0.47	0.37	0.44	0.42	0.44
	RMSE	48.11	80.28	59.02	47.32	76.51	79.05	37.68

NMB	1.29	0.29	5.14	0.20	1.78	1.77	0.59
NME	79.03	160.88	90.34	81.64	190.27	187.65	77.34
BIAS	-3.60	41.08	11.83	11.33	32.97	51.26	21.08
NSD	7.97	19.68	11.53	3.72	5.72	6.61	1.94

The calculation of the threshold velocity (u_{*t}) is based on dust particle size, following Shao and Lu (2000) (SL) in the present CMAQ version. According to the source code, the dust is divided into 4 particle sizes depending on soil texture types, namely coarse sand, fine-medium sand, silt, clay. Table S2 provides the values of u_{*t} from SL scheme and constants in earlier CMAQ version. It shows significant differences between these two methods, and considering the main erodible land-use types are cropland and barren land in Northeastern China, the u_{*t} from SL is generally 1~3 times larger than the constant u_{*t} except the soil texture of silt. This would lead to large discrepancies when calculating the dust horizontal flux.

Table S9 Threshold friction velocity (m s^{-1}) from Shao and Lu scheme and constants in earlier CMAQ version

Mean mass median particle diameter (m)	Description	Shao and Lu, 2000	u_{*t} constants		
			shrubland	shrubgrass land	barren land/cropland
6.90×10^{-4}	Coarse sand	0.427	0.34	0.34	0.23
2.10×10^{-4}	Fine-medium sand	0.250	0.47	0.47	0.24
1.25×10^{-4}	Silt	0.214	0.22	0.22	0.71
2.00×10^{-6}	Clay	0.910	0.42	0.42	0.29

References

Bagnold, R. A.: The physics of blown sand and desert dunes, Chapmann and Hall, Methuen, London, 265 pp., 1941.

Cakmur, R. V., R. L. Miller, and O. Torres: Incorporating the effect of small-scale circulations upon dust emission in an atmospheric general circulation model, J. Geophys. Res., 109, D07201, https://doi.org/10.1029/2003JD004067, 2004.

Fécan, F., Marticorena, B., and Bergametti, G.: Parametrization of the increase of the aeolian erosion threshold wind friction velocity due to soil moisture for arid and semi-arid areas, Ann. Geophys., 17, 149–157, https://doi.org/10.1007/s00585-999-0149-7, 1999.

Foroutan, H., Young, J., Napelenok, S., Ran, L., Appel, K. W., Gilliam, R. C. and Pleim, J. E.: Development and evaluation of a physics‐based windblown dust emission scheme implemented in the CMAQ modeling system, J. Adv. Model. Earth Syst., 9(1), 585–608, https://doi.org/10.1002/2016MS000823, 2017.

Ginoux, P., Chin, M., Tegen, I., Prospero, J. M., Holben, B., Dubovik, O. and Lin, S.: Sources and distributions of dust aerosols simulated with the GOCART model, J. Geophys. Res. Atmos., 106(D17), 20255–20273, https://doi.org/10.1029/2000JD000053, 2001.

Iversen, J. D. and White, B. R.: Saltation threshold on earth, mars and venus, Sedimentology, 29(1), 111–119, https://doi.org/10.1111/j.1365-3091.1982.tb01713.x, 1982.

Klingmüller, K., Metzger, S., Abdelkader, M., Karydis, V. A., Stenchikov, G. L., Pozzer, A. and Lelieveld, J.: Revised mineral dust emissions in the atmospheric chemistry–climate model EMAC (MESSy 2.52 DU_Astitha1 KKDU2017 patch), Geosci. Model Dev., 11, 989–1008, https://doi.org/10.5194/gmd-11-989-2018, 2018.

Klose, M., Shao, Y., Li, X., Zhang, H., Ishizuka, M., Mikami, M., and Leys, J. F.: Further development of a

parameterization for convective turbulent dust emission and evaluation based on field observations, J. Geophys. Res.-Atmos., 119, 10441–10457, https://doi.org/10.1002/2014JD021688, 2014.

Louis, J. F.: A parametric model of vertical eddy fluxes in the atmosphere. Boundary-Layer Meteorology, 17(2), 187-202, https://doi.org/10.1007/bf00117978, 1979.

Marticorena, B. and Bergametti, G.: Modeling the atmospheric dust cycle: 1. Design of a soil-derived dust emission scheme, J. Geophys. Res.-Atmos., 100, 16415–16430, https://doi.org/10.1029/95JD00690, 1995.

Marticorena, B., Bergametti, G., Aumont, B., Callot, Y., N'doumé, C., and Legrand, M.: Modeling the atmospheric dust cycle: 2. Simulation of Saharan dust sources, J. Geophys. Res.-Atmos., 102, 4387–4404, https://doi.org/10.1029/96JD02964, 1997.

Pryor, S., J. Schoof, and R. Barthelmie: Empirical downscaling of wind speed probability distributions, J. Geophys. Res., 110, D19109, https://doi.org/10.1029/2005JD005899, 2005.

Raupach, M. R., D. A. Gillette, and J. F. Leys: The effect of roughness elements on wind erosion threshold, J. Geophys. Res., 98(D2), 3023–3029, https://doi.org/10.1029/92JD01922, 1993.

Raupach, M.: Drag and drag partition on rough surfaces, Bound.- Lay. Meteor., 60, 375–395, https://doi.org/10.1007/BF00155203, 1992.

Shao, Y. and Lu, H.: A simple expression for wind erosion threshold friction velocity, J. Geophys. Res. Atmos., 105(D17), 22437–22443, https://doi.org/10.1029/2000JD900304, 2000.

Shao, Y., Ishizuka, M., Mikami, M. and Leys, J. F.: Parameterization of size‐resolved dust emission and validation with measurements, J. Geophys. Res. Atmos., 116(D8), https://doi.org/10.1029/2010JD014527, 2011.

Shao, Y.: A model for mineral dust emission, J. Geophys. Res. Atmos., 106(D17), 20239–20254, https://doi.org/10.1029/2001JD900171, 2001.

Shao, Y.: Simplification of a dust emission scheme and comparison with data, J. Geophys. Res. Atmos., 109(D10), https://doi.org/10.1029/2003JD004372, 2004.

White, B. R.: Soil transport by winds on Mars, J. Geophys. Res. Solid Earth, 84(B9), 4643–4651, https://doi.org/10.1029/JB084iB09p04643, 1979.